has neglected the energy of transfer of the solvated zwitterion from the gas phase into aqueous solution.

Guthrie[41] has applied Marcus theory to carbonyl hydrations and has found that observed rate constants for uncatalyzed hydration may be correlated satisfactorily with equilibrium constants for formation of a zwitterionic adduct but not with equilibrium constants for neutral adduct formation by a concerted mechanism. He argued that uncatalyzed hydration of carbonyl compounds generally proceeds by a stepwise mechanism involving rate-determining formation of a zwitterionic adduct followed by fast proton transfer to yield the neutral product; the concerted mechanism would become important only for extremely unreactive compounds. The present calculations for solvated zwitterions consider only the overall energy change in forming a zwitterionic intermediate, and no information is available concerning the energy barrier to this process. However, if this rate-determining transition state involves the same number of water molecules as does the solvated zwitterion, then the four-water solvated zwitterion may represent a good model for such an intermediate. This model would predict an additional three molecules of water associated with the transition state as over the doubly solvated reactant formaldehyde, in accord with the findings of Bell and his coworkers[28,29,31,32] (in aprotic solvents).

Funderburk, Aldwin, and Jencks,[43] in contrast, have given an argument for concerted, nonbifunctional uncatalyzed hydration proceeding by the equivalent of general-base catalysis. They have pointed out that observed rate constants for uncatalyzed (i.e., water catalyzed) formaldehyde hydration (and hemiacetal formation) lie nearer to the extrapolated Brønsted line for general-base catalysis than for general-acid catalysis. They have also pointed out that bifunctional catalysis by water cannot be important since there is no significant positive deviation of points for catalysis by carboxylate anions that cannot act as bifunctional catalysts. These authors concluded that uncatalyzed formaldehyde hydration represents general-base catalysis by water, possibly by means of a one-encounter involving a cyclic structure (cf. Figure 7) but not involving synchronous proton transfers in a fully concerted mechanism. Furthermore, it was argued that a zwitterionic intermediate has such a short lifetime that general catalysis is enforced and that the processes of HAR and PT must be coupled in a concerted mechanism.

(43) Funderburk, L. H.; Aldwin, L.; Jencks, W. P. *J. Am. Chem. Soc.* **1978**, *100*, 5444-5459.

Summary

Gas-phase formaldehyde hydration is probably a termolecular reaction proceeding by means of a concerted mechanism involving FW2‡. The single ancillary water molecule has a dramatic effect that may be understood in terms of a strong hydrogen-bonding interaction between the bifunctional catalyst and the (unbound) zwitterionic adduct of the nucleophilic water with formaldehyde.

In aprotic solvents, carbonyl addition probably involves three molecules of water in a cyclic transition state rather than just two as in FW2‡. As yet the structure of this transition state in unknown, and it is unclear whether the mechanism is fully concerted (involving synchronous motions of all the transferring protons) or "intimate stepwise" (involving at least two steps but occurring within a single encounter; one of the steps may involve coupled HAR and PT as in general acid-base catalysis). A theoretical study of the system $3H_2O + CH_2O$ is in progress in our laboratories.

In aqueous solution it is not all clear whether the mechanism is stepwise (involving a solvated zwitterion) or concerted. It may be that not just a single mechanism is involved but that several competing mechanisms may be significant. Analysis of the experimental kinetic data is not a simple matter and may perhaps be assisted by evidence from appropriate theoretical studies of model systems.

Acknowledgment. This work is supported in part by grants from the National Institute of General Medical Sciences (R01-GM-20198) and by the National Resource for Computation in Chemistry under grants from the National Science Foundation (CHE-7721305) and the Office of Basic Energy Sciences of the United States Department of Energy (W-7405-NG-48). We also express our appreciation for the assistance provided by the respective computer centers of the Universities of Kansas and Cambridge.

Electronic Interactions in Mixed-Valence Molecules As Mediated by Organic Bridging Groups

David E. Richardson and Henry Taube*

Contribution from the Department of Chemistry, Stanford University, Stanford, California 94305. *Received March 16, 1982*

Abstract: The preparations, spectroscopic properties, and electrochemistry of a number of new complexes with the general formula $[(Ru(NH_3)_5)_2L]^{n+}$ (n = 4, 5, 6) are reported, where L is a rigid organic bridging ligand (including pyrimidine, the dicyanobenzenes, 3- and 4-cyanopyridine, and dicyanonaphthalenes). These complexes and others are used to illustrate several aspects of the effect of bridging ligand structure on metal-metal interactions in polymetallic systems. The observed trends are predicted theoretically by combining a molecular orbital description of the bridging ligand with a semiempirical measure of metal-ligand charge-transfer interactions. The relationship of bridging ligand size, orientation of substituents, interplanar distances, and saturation to metal-metal interaction is demonstrated both theoretically and experimentally. Bridging ligand effects in intramolecular electron transfer are considered in the context of nonadiabatic theories and electronic interactions between redox sites. The relationship between the characteristics of the bridging group and the comproportionation constant, K_c, is discussed.

Numerous binuclear mixed-valence (MV) complexes based on ruthenium ammines have been reported[1-10] since the synthesis of the Creutz ion, $[(Ru(NH_3)_5)_2pyrazine]^{5+}$.[11] Examples of both localized[2-5,10,12] and delocalized (valence averaged)[1,8,9] systems

(1) Richardson, D. E.; Sen, J.; Buhr, J. D.; Taube, H. *Inorg. Chem.* **1982**, *21*, 3136.
(2) Sutton, J. E.; Taube, H. *Inorg. Chem.* **1981**, *20*, 3125.
(3) (a) Stein, C. A.; Taube, H. *J. Am. Chem. Soc.* **1981**, *103*, 693. (b) Stein, C. A.; Taube, H. Ibid. **1978**, *100*, 1635.
(4) Tanner, M.; Ludi, A. *Inorg. Chem.* **1981**, *20*, 2348.

0002-7863/83/1505-0040$01.50/0

have been examined spectroscopically and electrochemically. The physical description of the Creutz ion[11] remains controversial.[13] General trends have been observed in the dependence of the properties of the MV ions on the structure of the bridging group. For example, strong metal–metal interactions are found to occur with small, symmetrical bridging ligands such as dinitrogen,[1] dicyanogen,[9] and pyrazine.[11] Larger aromatic ligands (such as bipyridines)[2,4,10] and saturated ligands (e.g., dithianes)[3] result in relatively weak metal–metal interactions and valence-localized MV ions.

We have been interested in defining more clearly the relationship between the bridging ligand structure and the magnitude of the interaction between the metal centers. One of the most sensitive and direct probes of metal–metal interaction in MV compounds is the intervalence transfer (IT) band[14-17] usually found in the near-IR for ruthenium ammine complexes. Numerous studies have been devoted to the correlation of molecular structure with IT band energies and shapes, but few workers have focused on the band intensities even though it is the band intensities in localized MV compounds that are directly related to the metal–metal interactions.[14,15]

We report here a number of new complexes of the general formula $[(Ru(NH_3)_5)_2L]^{n+}$ (n = 4, 5, 6) where L is a rigid bifunctional organic bridging ligand. While individual members of this series hold no special interest, the trends in properties observed for the group are instructive. In addition, we have applied a theoretical method based on the earlier work by Mayoh and Day[18-20] to rationalize the observed trends.

The electrochemistry of these ions has been investigated, and the working curves reported elsewhere[12] have been used to evaluate the comproportionation constants, K_c, for the equilibrium of eq 1. Applications of the results for the MV complexes to intra-

$$[Ru^{II}Ru^{II}]^{4+} + [Ru^{III}Ru^{III}]^{6+} \rightleftarrows 2[Ru^{II}Ru^{III}]^{5+} \quad (1)$$

molecular electron transfer reactions are also discussed.

Experimental Section

Reagents and Materials. Argon (99.995%, Liquid Carbonic) was deoxygenated by passing it through two chromous ion scrubbing towers. The output gas was passed through a water bubbler for applications to aqueous solutions or through concentrated sulfuric acid and then dried acetone for acetone solutions. House distilled water was purified by redistillation from alkaline permanganate in an all-glass still. Deuterium sulfate was purchased from ICN and diluted with D_2O (MSD Isotopes, Merck) to the desired concentration.

Trifluoromethanesulfonic acid was purchased from 3M (product name Fluorad). It was purified by distillation under vacuum in an ungreased apparatus and the clear distillate was diluted to ~6 M immediately after distillation. This stock solution was titrated against sodium hydroxide and diluted to the desired concentration. Sephadex SP-C25-120 (Sigma) was washed and stored under distilled water for at least a day before use. The packed Sephadex columns were washed with 2 M HCl, then distilled water. Aluminum oxide 90 active (neutral, acidity I, EM Reagents) was stirred in chloroform/methanol to charge the column. A UV lamp was used to locate organic bands.

Organic Ligands. Pyrimidine, 1,2-dicyanobenzene, and 3-cyanopyridine were purchased from Aldrich and used as supplied. The ligands 4-cyanopyridine, 1,3-dicyanobenzene, and 1,4-dicyanobenzene were purchased from Aldrich and recrystallized at least 2 times from ethanol.

Five isomers of dicyanonaphthalene were synthesized following literature procedures.[21-23] Purity was confirmed by comparison of melting points to the literature values, elemental analysis, and gas chromatography.

Pseudo-*p,p'*-dicyano[2.2]paracyclophane was prepared by a procedure based on the report of Reich and Cram.[24] The intermediate pseudo-*p,p'*-dibromo[2.2]paracyclophane was prepared by direct bromination of [2.2]paracyclophane (Aldrich). The dicyano derivative was prepared by heating 0.5 g (1.4 mmol) of the dibromo with 0.3 g (3.4 mmol) of technical cuprous cyanide in a few milliliters of quinoline. Heat was applied by a sodium nitrite/potassium nitrate (1:1) salt bath at 240 °C. An argon atmosphere was supplied and sufficient pyridine was added to cause refluxing. After 24 h, the hot reaction mixture was stirred into 50 mL of 15% ammonium hydroxide and 50 mL of dichloromethane. The organic layer was separated and washed with 15% ammonium hydroxide, water, three portions of 6 N HCl, saturated sodium bicarbonate solution, and saturated sodium chloride solution. After drying and removing the solvent, the crude product was chromatographed on a 3 × 6 cm alumina column. The desired isomer was eluted with 40% ether–pentane. Two recrystallizations from ethanol gave a white solid, mp 235–239 °C (lit.[24] mp 237.5–239 °C).

The intermediate 1,3-dibromoadamantane and the ligand 1,3-dicyanoadamantane were generously provided by Daniel Geselowitz. For the preparation of the latter, about 1 g of dibromoadamantane (prepared by the method of Baughman)[25] and 0.7 g of cuprous cyanide were mixed and heated in as 25-mL round-bottom flask capped with a drying tube. A fused salt bath was used and was kept at 250 °C. After 2 h, the flask was oriented to allow sublimation to the neck of the flask. The flask was cooled and the sublimed product was recovered (yield ca. 0.5 g) and recrystallized from large volumes of petroleum ether, yielding colorless needles, mp 196.5–197.5 °C. Anal. Calcd for $C_{10}H_{12}N_2$: C, 77.38; H, 7.58; N, 15.04. Found: C, 77.12; H, 7.25; N, 14.80.

Mononuclear Ruthenium Complexes. The starting material for all syntheses was hexaammineruthenium(III) chloride (Matthey Bishop). The hexaammine was converted to chloropentaammineruthenium(III) chloride by the procedure of Vogt et al.[26]

The white solid $[Ru(NH_3)_5H_2O](CF_3SO_3)_3$ was synthesized by the procedure of Krentzien,[27] and $[Ru(NH_3)_5H_2O](PF_6)_2$ was synthesized by the procedure of Sutton.[28]

The complex $[Ru(NH_3)_5L](PF_6)_2$[29] (L = pyrimidine) was prepared by dissolving 0.1 g of $[Ru(NH_3)_5H_2O](PF_6)_2$ under argon in 5 mL of acetone which contained 0.1 g of pyrimidine. After 30 min, LiBr was added to precipitate the red bromide salt. The crude bromide was reprecipitated as the hexafluorophosphate salt, and this was recrystallized once from a minimum of warm water. The solid was washed with ethanol and dried under vacuum desiccation.

The complexes $[Ru(NH_3)_5L](ClO_4)_2$ (L = 1,4 dicyanobenzene and benzonitrile) were synthesized by the method of Ford.[30] Purity was confirmed by comparing the spectra with those published.[30] The CN-bound cyanopyridine complexes $[Ru(NH_3)_5L](ClO_4)_2$ were synthesized by the method of Ford.[31] Purity was confirmed by spectra and cyclic voltammetry.

Binuclear Ruthenium Complexes. Binuclear complexes prepared for this study were synthesized by one or both of two techniques. All preparations were done in the dark under an argon atmosphere. Method 1: in some cases, it sufficed to treat the ligand in ~5 mL of ethanol with 2 equiv of $[Ru(NH_3)_5H_2O]^{2+}$ in ~10 mL of water (from reduction of 150 mg of $Ru(NH_3)_5Cl_3$ by Zn/Hg) for several hours. Addition of a suitable counterion precipitated the [II, L, II] complex (see ref 32 for glossary of abbreviations). Method 2: for some ligands, pyrimidine in particular, water was not a satisfactory solvent. In those cases, acetone was used, thereby increasing the rate of binuclear formation. The ligand

(5) Sutton, J. E.; Sutton, P. M.; Taube, H. *Inorg. Chem.* **1979**, *18*, 1017.
(6) Taube, H. *Ann. N.Y. Acad. Sci.* **1978**, *313*, 481.
(7) von Kameke, A.; Tom, G. M.; Taube, H. *Inorg. Chem.* **1978**, *17*, 1790.
(8) Krentzien, H.; Taube, H. *J. Am. Chem. Soc.* **1976**, *98*, 6379.
(9) Tom, G. M.; Taube, H. *J. Am. Chem. Soc.* **1975**, *97*, 5310.
(10) Tom, G. M.; Creutz, C.; Taube, H. *J. Am. Chem. Soc.* **1974**, *96*, 7827.
(11) (a) Creutz, C.; Taube, H. *J. Am. Chem. Soc.* **1973**, *95*, 1086. (b) Creutz, C.; Taube, H. *Ibid.* **1969**, *91*, 3988.
(12) Richardson, D. E.; Taube, H. *Inorg. Chem.* **1981**, *20*, 1278.
(13) Day, P. *Int. Rev. Phys. Chem.* **1981**, *1*, 149.
(14) Hush, N. S. *Electrochim. Acta* **1968**, *13*, 1005.
(15) Hush, N. S. *Prog. Inorg. Chem.* **1967**, *8*, 391.
(16) Robin, M. B.; Day, P. *Adv. Inorg. Radiochem.* **1967**, *10*, 247.
(17) Wong, K. Y.; Schatz, P. N. *Prog. Inorg. Chem.* **1981**, *28*, 369.
(18) Mayoh, B.; Day, P. *Inorg. Chem.* **1974**, *13*, 2273.
(19) Mayoh, B.; Day, P. *J. Am. Chem. Soc.* **1972**, *94*, 2885.
(20) Mayoh, B.; Day, P. *J. Chem. Soc., Dalton Trans.* **1974**, 846.
(21) Bradbrook, E. F.; Linstead, R. P. *J. Chem. Soc.* **1936**, 1739.
(22) King, H.; Wright, E. V. *J. Chem. Soc.* **1939**, 253.
(23) Richardson, D. E. Ph.D. Thesis, Stanford University, 1981.
(24) Reich, H. J.; Cram, D. J. *J. Am. Chem. Soc.* **1969**, *91*, 3527.
(25) Baughman, G. L. *J. Org. Chem.* **1964**, *29*, 238.
(26) Vogt, L.; Katz, J.; Wiberly, S. *Inorg. Chem.* **1965**, *4*, 1157.
(27) Krentzien, H. Ph.D. Thesis, Stanford University, 1976.
(28) Sutton, J. E. Ph.D. Thesis, Stanford University, 1979.
(29) Ford, P.; Rudd, DeF. P.; Gaunder, R.; Taube, H. *J. Am. Chem. Soc.* **1968**, *90*, 1187.
(30) Clarke, R. E.; Ford, P. C. *Inorg. Chem.* **1970**, *9*, 227.
(31) Clarke, R. E.; Ford, P. C. *Inorg. Chem.* **1970**, *9*, 495.
(32) The notations [II, L, II], [II, L, III], and [III, L, III] are used to indicate overall oxidation states for the binuclear complexes with bridging ligand L. Abbreviations used here for L are: pyrazine, pyz; pyrimidine, pym; 1,2-dicyanobenzene, 12DCB; 1,3-dicyanobenzene, 13DCB; 1,4-dicyanobenzene, 14DCB; 3-cyanopyridine, 3CP; 4-cyanopyridine, 4CP; *i,j*-dicyanonaphthalene, *ij*DCN; 1,3-dicyanoadamantane, 13DCA; pseudo-*p*-dicyano[2.2]paracyclophane, PPDCP; 1,4-dicyanobicyclo[2.2.2]octane, DCBCO.

was treated with a slight excess of $[Ru(NH_3)_5H_2O](PF_6)_2$ (~150 mg) and addition of saturated LiBr after a few hours gave the crude bromide salt. The crude product was purified by inert-atmosphere ion-exchange chromatography.

Details for each preparation follow. The products were stored under vacuum desiccation. Microanalyses are given in the Results section.

(μ-Pyrimidine)bis(pentaammineruthenium(II)) Hexafluorophosphate Hydrate. The crude bromide of method 2 was chromatographed on Sephadex. Elution with 0.3 M HCl removed the mononuclear pyrimidine complex and unreacted $[Ru(NH_3)_5H_2O]^{2+}$. The binuclear complex was removed with 0.5 HCl, and the eluent was added to a large quantity of acetone, which precipitated a red solid. The crude chloride salt was dissolved on a small amount of water and reduced over Zn/Hg with argon bubbling for 15 min. Addition of NH_4PF_6 gave a red precipitate which was collected and washed with ethanol and ether. The solid is stable for several weeks in a vacuum desiccator.

(μ-Pyrimidine)bis(pentaammineruthenium(III)) Chloride. The crude bromide salt obtained directly from acetone in the above preparation was dissolved in small volume of 1 M HCl. The complex was oxidized by dropwise addition of ceric solution with stirring. This resulting pinkish yellow solution was diluted with 10 volumes of water and chromatographed on Sephadex. Elution with 0.75 M HCl removed the pink impurity, and 1.0 M HCl eluted the yellow binuclear band. This 1.0 M HCl eluent was kept frozen overnight. Thawing revealed small yellow crystals, which were collected and washed with ethanol and ether. The resulting yellow solid is stable for at least several weeks under vacuum desiccation.

$[(Ru(NH_3)_5)_2L]X_4$ (L = 1,4-Dicyanobenzene, 1,3-Dicyanobenzene, or 1,2-Dicyanobenzene). Binuclear complexes of the dicyanobenzenes were originally prepared by Krentzien.[27] The red salt $[(Ru(NH_3)_5)_214DCB](CF_3SO_3)_4$ was prepared by method 1 with addition of 5 M CF_3SO_3H to the filtered reaction solution. The resulting crystals were washed with ethanol and ether.

The yellow salt $[(Ru(NH_3)_5)_213DCB](CF_3SO_3)_4$ was prepared by method 1, except $[Ru(NH_3)_5H_2O](CF_3SO_3)_3$ was the starting material. The filtered reaction solution was evaporated until crystals precipitated. The yellow salt $[(Ru(NH_3)_5)_213DCB](BF_4)_4$ was also prepared by method 1 where $NaBF_4$ was added to precipitate the solid. Both products were washed with ethanol and ether. Some discoloration was observed after several days under vacuum desiccation.

The orange salt $[(Ru(NH_3)_5)_212DCB]Br_4$ was prepared by method 1 with KBr added to precipitate the solid.

(μ-3-Cyanopyridine)bis(pentaammineruthenium(II)) Hexafluorophosphate. This complex was prepared by method 1 with NH_4PF_6 to precipitate the yellow salt, which was washed with ethanol and ether. Method 2 produced a mixture of monomers and the binuclear complex. These were cleanly separated on Sephadex and the products were identified by cyclic voltammetry. The 0.3 M HCl fraction was pyridine bound, the 0.4 M HCl fraction was CN bound, and the binuclear complex was eluted with 0.5 M HCl. The binuclear fraction was reduced over Zn/Hg for 20 min, and a yellow solid was precipitated by addition of NH_4PF_6. The product was washed with ethanol and ether.

(μ-4-Cyanopyridine)bis(pentaammineruthenium(II)) Perchlorate. This red solid could be prepared in water or acetone. For method 1, $NaClO_4$ was used to precipitate the complex. For method 2, the 0.5 M HCl fraction from Sephadex was saturated with $NaClO_4$ and refrigerated overnight to yield a fine, dark purple solid. The perchlorate decomposes over a period of 1–2 months under vacuum, turning black.

Dicyanonaphthalene Binuclear Ruthenium(II) Complexes. Five complexes of formula $[(Ru(NH_3)_5)_2L]X_4$ (L = 15DCN, 16DCN, 17DCN, 26DCN, and 27DCN) were synthesized by method 2 followed by chromatography under argon on Sephadex. After complete elution of monomeric species with 0.4 M HCl, the binuclear complex was eluted with 1 M HCl. In many cases, products identified as trinuclear complexes were retained at the top of the column and could be eluted with 2 M HCl.

The binuclear complexes were isolated as solids in different ways. For 15DCN, 17DCN, and 26DCN, addition of solid $NaClO_4$ (to saturate) followed by refrigeration overnight gave dark solids which were collected by filtration. The 17DCN binuclear species was isolated by freeze drying the eluent to about $^1/_2$ volume and precipitating the chloride by adding acetone. The chloride was redissolved in water and addition of $NaClO_4$ gave a dark solid. The 27DCN binuclear species was precipitated with KI from the 1 M HCl fraction by cooling on ice for several hours, giving a reddish powder. All solid products were washed with ethanol and ether and stored in a vacuum desiccator. After 1 month, varying degrees of decomposition were obvious in all but the 26DCN product, which is stable for many months.

(μ-Pseudo-p,p'-dicyanoparacyclophane)bis(pentaammineruthenium(II)) Bromide. Exactly 9.60 mg of PPDCP (0.0372 mmol) was dissolved in acetone and the solution saturated with argon; thereupon 37.2 mg of $[Ru(NH_3)_5H_2O](PF_6)_2 \cdot H_2O$ (0.0744 mmol) was added and the reaction was allowed to proceed under argon for 1 h. The volume of acetone was reduced to 2 mL by flushing with dry argon, and LiBr was added; a red solid precipitated which was washed with acetone and ether. The scarcity of this ligand precluded purification of the bromide salt by chromatography; however, the analysis C/H and C/N ratios showed the binuclear complex to be the major constituent of the solid.

(μ-1,3-Dicyanoadamantane)bis(pentaammineruthenium(II)) Perchlorate. Following method 2, the crude product was chromatographed on Sephadex. Elution with 0.3 M HCl gave first a light pink band followed by a yellow band. The latter proved to be the binuclear complex, which was precipitated by adding $NaClO_4$ to the eluent. The yellow solid was collected and washed with ethanol and ether.

Instrumentation and Techniques. Ultraviolet, visible, and near-IR spectra were recorded at 25 ± 0.5 °C with a Beckman Model 5270 spectrophotometer equipped with a thermostated cell holder. Infrared spectra (200–4000 cm^{-1}) were recorded with a Perkin-Elmer Model 621 instrument. Samples were prepared for IR spectra as KBr pellets (2–3% sample by weight). Electrochemical instrumentation and techniques are described elsewhere.[13] All elemental analyses were performed by the Stanford University Microanalytical Laboratory.

Table I. Elemental Analyses of Ruthenium Complexes

formula (R ≡ $(Ru(NH_3)_5)$)		% C	% H	% N	% Ru
$[Ru(NH_3)_5pym](PF_6)_2$	calcd:	8.64	3.44	17.62	18.17
	found:	8.74	3.50	17.45	18.4
$[R_2pym](PF_6)_4 \cdot H_2O$	calcd:	4.57	3.45	15.98	19.2
	found:	4.88	3.50	15.84	19.3
$[R_2pym]Cl_6 \cdot H_2O$	calcd:	7.03	5.31	24.60	
	found:	6.70	5.21	23.06	
$[R_23CP](PF_6)_4$	calcd:	6.82	3.25	15.91	
(acetone prep)	found:	6.77	3.19	15.88	
(water prep)	found:	6.91	3.12	15.49	
$[R_24CP](ClO_4)_4$	calcd:	8.24	3.92	19.21	
(acetone prep)	found:	8.67	3.97	18.51	
(water prep)	found:	8.53	3.55	17.83	
$[R_212DCB]Br_4$	calcd:	11.72	4.18	20.48	
	found:	10.97	3.92	18.84	
$[R_213DCB](ClO_4)_4$	calcd:	10.70	3.81	18.70	
	found:	10.97	3.95	17.76	
$[R_213DCB](BF_4)_4$	calcd:	11.34	4.04	19.80	
	found:	11.25	3.81	19.00	
$[R_214DCB](CF_3SO_3)_4$	calcd:	13.14	3.12	15.32	
	found:	12.96	3.07	14.81	
$[R_215DCN](ClO_4)_4 \cdot H_2O$	calcd:	14.91	3.96	17.38	
	found:	14.81	3.93	17.73	
$[R_216DCN](ClO_4)_4$	calcd:	15.20	3.83	17.71	
	found:	15.38	3.58	15.77	
$[R_217DCN](ClO_4)_4$	calcd:	15.20	3.83	17.71	
	found:	15.72	3.47	16.16	
$[R_226DCN](ClO_4)_4$	calcd:	15.20	3.83	17.71	
	found:	15.69	3.95	17.40	
$[R_227DCN]I_4$	calcd:	13.62	3.43	15.88	
	found:	13.92	3.40	14.79	
$[R_213DCA](ClO_4)_4$	calcd:	15.04	4.63	17.53	
	found:	14.85	4.41	16.37	
$[R_2PPDCP]Br_4$	calcd:	22.75	4.67	17.68	
	found:	21.32	4.55	15.28	

Results

Microanalyses. Elemental analyses for ruthenium complexes synthesized for this study are summarized in Table I. As found by Sutton,[28] microanalyses for nitrogen tend to be unreliable for the binuclear complexes of ruthenium ammines, even though carbon and hydrogen are found to be correct within experimental error. The low nitrogen analyses are often taken as evidence for replacement of ammonia by water in the ruthenium inner coordination sphere, and it was necessary to determine whether this was actually the case here. The presence of water bound to ruthenium(II) can be detected easily in cyclic voltammetry by adding acetonitrile to the electrolyte ($E_{1/2}$ for the resulting acetonitrile complex will then appear about 200 mV more positive than for the aquo species). Due to the high affinity of acetonitrile for ruthenium(II), virtually all aquo species will be converted to the nitrile, thus quantitative estimates of the loss of ammonia can be made. The binuclear complexes in Table I were all found to have less than 5% of the acetonitrile complex, which is the limit

Table II. Ultraviolet–Visible Spectra of Ruthenium Binuclear Complexes[a]

	$n = 4$		$n = 5$		$n = 6$	
ligand	ν_{max}[b]	$\epsilon/10^3$[c]	ν_{max}[b]	$\epsilon/10^3$[c]	ν_{max}[b]	$\epsilon/10^3$[c]
pym	22.2	14.8	21.9	6.84	35.3	4.66
	39.2	1.41	36.4	3.02	44.8	6.99
	42.7	7.50	43.1	6.40		
3CP	23.9	13.7	22.8	8.25	25.6	1.87
	39.2	19.5	39.0	17.0	38.9	8.10
	46.5	11.8				
4CP	19.3	18.0	20.3	10.3	29.2	4.33
	39.5	13.5			39.2	6.33
	46.1	11.0			36.4	5.66
12DCB	23.8	11.8	22.5	4.6	25.6 sh	2.27
	38.5	19.7	38.5		34.5	6.26
13DCB	24.7	19.1	24.6	8.72	25.6 sh	
	39.2	30.2	39.2	21.6	39.5	14.5
	43.9	24.7	43.9	23.3		
14DCB	21.8	26.7	21.5	13	34.4	14.7
	38.9	32.8	39.0		42.9	14.1
15DCN	21.7	13.8	21.7		25.6 sh	1.99
	35.2	19.5	33.3		29.8	13.6
	39.7	23.2	44.4		31.9	15.2
	45.1	49.9			43.5	44.3
16DCN	23.5	6.77			25.6 sh	1.27
	33.3 sh	7.55			43.7	26.9
	43.1	29.4				
	41.7	27.5				
17DCN	22.6	8.74	22.2		25.0 sh	2.0
	34.5 sh	11.7	42.1		32.0	11.2
	41.7	38.3			42.6	33.8
26DCN	21.9	12.1	21.9		25.0	3.0
	27.6	6.5	41.3		28.6 sh	6.8
	29.0	6.8			33.0	17.0
	41.3	58.1				
27DCN	23.2	18.9	23.2		20.4 sh	
	43.9	52.7	43.9		43.9	52.6
PPDCP	24.6	8.5				
	42.0	20.3				

[a] Molecular formula $[(Ru(NH_3)_5)_2\text{ligand}]^{n+}$ where $n = 4$, 5, and 6. Taken in 1 M H_2SO_4 at room temperature. Spectra of oxidized forms ($n = 5$, 6) obtained by ceric oxidation of $n = 4$ species. [b] Band maxima in $cm^{-1} \times 10^3$. [c] Extinction coefficients in M^{-1} cm^{-1}. Where given for $n = 5$, intensities are not corrected for comproportionation.

of detection. We therefore assume the nitrogen analyses are in error and base judgments of analytical purity on carbon and hydrogen analyses. In addition, the absence of spurious peaks in the cyclic voltammograms can be used to rule out the presence of unreacted $[Ru(NH_3)_5H_2O]^{2+/3+}$ and multiply substituted ruthenium (e.g., $[Ru(NH_3)_4L_2]^{2+}$).

UV–Vis Spectra of Binuclear Complexes. The electronic spectra in the UV–Vis range of the binuclear complexes $[(Ru(NH_3)_5)_2L]^{n+}$ ($n = 4$, 5, 6) are summarized in Table II. For comparison, spectra of several mononuclear complexes are given in Table III, and UV spectra of the bridging ligands are given in Table IV. (Complete spectral traces are given elsewhere.[23]) In all cases, the $n = 4$ spectra were obtained by dissolving the solids in deaerated 1 M H_2SO_4 or D_2SO_4/D_2O. The [II, L, II] solution was then oxidized by adding aliquots of Ce(IV) in 1 M H_2SO_4 or D_2SO_4/D_2O to give the [II, L, III] ($n = 5$) solution and finally the [III, L, III] ($n = 6$). As found for other weakly coupled mixed-valence dimers,[28] correcting the $n = 5$ spectra for comproportionation does not greatly alter the extinction coefficients.

In the [II, L, II] spectra ($n = 4$), Table II, two types of transitions are observed. One or more metal-to-ligand charge-transfer (MLCT) bands are found in the visible and ultraviolet regions. While the intensity in the visible region is predominantly due to MLCT (which obscures the relatively weak d–d transitions), the UV bands are usually composites of MLCT and ligand-centered transitions (Table IV).

With the exception of L = 4CP, the low-energy MLCT bands for the [II, L II] species are within 1000 cm^{-1} of the analogous

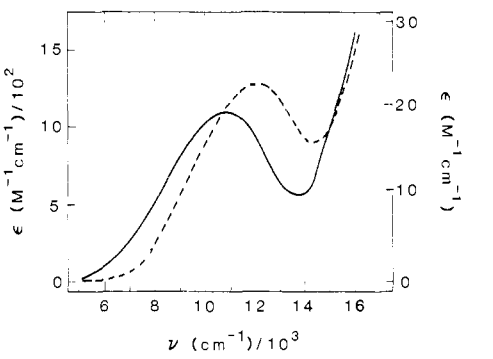

Figure 1. Near-IR spectrum of $[(Ru(NH_3)_5)_2L]^{5+}$ in 1 M D_2SO_4/D_2O. L = 4CP (solid line, left-hand scale), L = 3CP (dashed line, right-hand scale).

bands of the monomeric $[Ru(NH_3)_5L]^{2+}$ complexes (Table III), and the binuclear MLCT intensities are roughly twice the monomer intensities. The [II, 4CP, II] MLCT band at 19.3×10^3 cm^{-1} has a shoulder at $\sim 25 \times 10^3$ cm^{-1}, suggesting that the spectrum is dominated by the Ru(II)–pyridyl interactions, the shoulder being due to the Ru(II)–nitrile group (the $[Ru(NH_3)_5 4CP]^{2+}$ (CN bound) MLCT band is at 23.5×10^3 cm^{-1}.

The features of the spectra of the [III, L, III] complexes ($n = 6$) generally can be classified in three categories: (1) the lowest energy bands in the region $25–28 \times 10^3$ cm^{-1} are typically weak ($\epsilon \leq 1000$ M^{-1} cm^{-1} and probably originate from d–d transitions on Ru(III),[33] (2) between $30–35 \times 10^3$ cm^{-1}, intense transitions ($\epsilon > 5000$ M^{-1} cm^{-1}) are often found which are not associated with intraligand transitions and are assigned as LMCT transitions, (3) intraligand transitions are found at $\geq 35 \times 10^3$ cm^{-1}. For the dicyanonaphthalenes, the principal $\pi \rightarrow \pi^*$ transitions are intense ($\epsilon \sim 40\,000$ M^{-1} cm^{-1}) and change little from the [II, L, II] spectra.

The spectra of the [II, L, III] complexes ($n = 5$) are composites of the $n = 4$ and $n = 6$ spectra for the symmetrical bridging ligands. The MLCT intensities drop to about half the $n = 4$ values, and there is a trend toward lower energy for the MLCT band maxima. This shift is correlated with the increased π acidity of Ru(III)–L compared to Ru(II)–L and is most obvious when the bridge is relatively small (pym, 12DCB) rather than large (dicyanonaphthalenes). For the cyanopyridines, the shifts are complicated by the unsymmetrical nature of the bridge. The [II, 3CP, III] and [II, 4CP, III] binuclear species will have Ru^{II} bound to the nitrile group. For 4CP, the result is that the MLCT band shifts to higher energy than that of [II, 4CP, II] while the "normal" shift to lower energy is found for [II, 3CP, III].

Intervalence Bands. In all but two of the new mixed-valence complexes studied, bands are found in the near-IR region which are not present in the [II, L, II] or [III, L, III] complexes. On the basis of past experience, these transitions can be confidently assigned as intervalence transfer (IT) bands. These bands are essentially Ru(II) $\rightarrow$ Ru(III) charge-transfer transitions and achieve intensity in the present cases by bridge-mediated metal–metal interactions. The IT bands are usually found on the low-energy tail of the MLCT band in the visible region. Several examples are shown in Figures 1 and 2. For an estimate of the IT intensity, the base line is taken as the average of the [II, L, II] and [III, L, III] trace in the IT region. Positions, widths, and intensities are summarized in Table V. The intensities have been corrected by a factor of $(2 + (K_c)^{1/2})/(K_c)^{1/2}$ to account for comproportionation. Widths were usually obtained by doubling the half-width of the low-energy side of the band. When no distinct peak is resolved, widths and positions can only be approximated. No IT bands ($\epsilon \geq 5$ M^{-1} cm^{-1}) could be found for L = 16DCN or 27DCN.

The theoretical treatment of the intensities of the IT bands is deferred to the Discussion, but it seems worthwhile now to draw

(33) Guensburger, D.; Garnier, A.; Danon, J. *Inorg. Chem. Acta* **1977**, *21*, 119.

Table III. Visible Spectra of Pentaammineruthenium(II) Complexes[a]

ligand	ν_{max}/ ($cm^{-1} \times 10^3$)	$\Delta\nu_{1/2}$/ ($cm^{-1} \times 10^3$)	ϵ/(10^3 M^{-1} cm^{-1})	μ_{CT}/(e Å)	β_1/ ($cm^{-1} \times 10^3$)	Δ/ ($cm^{-1} \times 10^3$)	$\lvert a_N \rvert^g$
benzonitrile[b,c]	26.6	6.5	8.51	0.94	9.09	25.9	0.322
pyrimidine[b]	22.5	5.5	6.03	0.79	7.54	21.4	0.459
pyridine[d]	24.5	4.2	7.76	0.75	6.30	23.4	0.571
pyrazine[e]	21.2	5.1	13.3	1.15	7.78	19.1	0.578
13DCB[b,c]	24.8	5.0	12.3	1.02	9.91	24.3	0.250
14DCB[b,c]	21.6	5.0	13.6	1.16	10.08	20.8	0.287
3CP (CN bound)[b,f]	24.9	5.2	5.62	0.70	7.80	24.6	0.264
4CP (CN bound)[b,f]	23.5	4.6	5.37	0.66	5.81	23.2	0.316

[a] Molecular formula $[Ru(NH_3)_5L]^{2+}$. In water at room temperature. [b] This work. [c] Reference 30. [d] Reference 29. [e] Reference 11a. [f] Reference 31. [g] Coefficient of N orbital in the LUMO from INDO calculations (see reference 48).

Table IV. Ultraviolet Spectra of Bridging Ligands[a]

compd	ν_{max}/($cm^{-1} \times 10^3$) (ϵ/(10^3 M^{-1} cm^{-1}))
pym	21.7 (0.46), 40.9 (3.32)
3CP	36.9 (1.72), 37.7 (2.33), 38.6 (2.22), 46.1 (9.95)
4CP	36.8 (2.84), 45.5 (7.47), 47.3 (8.81)
12DCB	34.4 (1.70), 35.5 (1.66), 36.2 (1.12), 42.1 (10.5)
13DCB	34.7 (0.54), 35.7 (0.49), 36.8 (0.36), 48.8 (45.6)
14DCB	34.8 (0.54), 36.0 (1.78), 40.5 (22.4), 42.5 (22.3)
15DCN	30.5 (9.35), 32.0 (14.3), 32.3 (14.6), 33.4 (19.4), 34.8 (14.1), 43.9 (102.)
16DCN	29.9 (2.15), 31.3 (1.78), 33.2 (5.66), 33.9 (6.45) 34.6 (6.88), 35.2 (6.76), 41.8 (66.4), 43.1 (57.0)
17DCN	30.0 (1.78), 30.7 (1.28), 31.6 (2.47), 33.1 (8.44) 33.7 (8.88), 34.4 (8.09), 42.6 (64.1), 43.5 (59.2)
26DCN	30.3 (2.78), 33.8 (11.9), 35.2 (13.9), 36.5 (9.59) 41.3 (142.), 42.6 (68.8)
27DCN	29.9 (1.82), 31.2 (2.57), 33.0 (8.61), 33.6 (9.11) 34.4 (8.28), 41.8 (63.6), 43.3 (59.0)
13DCA	b
PPDCP	33.0 (1.80), 42.5 (15.8)

[a] In ethanol at room temperature except for 26DCN and 27DCN, in dichloromethane. [b] $\epsilon < 30$ down to 50.0×10^3 cm^{-1}.

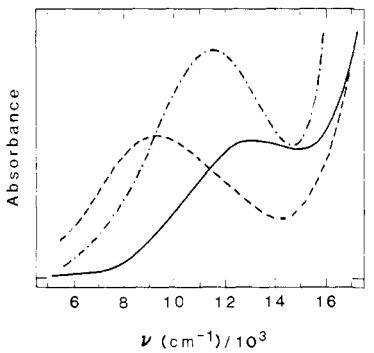

Figure 2. Near-IR spectrum of $[(Ru(NH_3)_5)_2L]^{5+}$ in 1 M D_2SO_4/D_2O. L = 13DCB (solid line), L = 12DCB (dash line), L = 14DCB (dash-dot line). Absorbance scale different for each spectrum.

attention to the important trends: (1) Within a series of isomers (L = pyrazine and pyrimidine; L = 1,2-, 1,3-, and 1,4-dicyanobenzene, etc.), the [II, L, III] complexes with the metals separated by an even number of conjugated atoms tend to have the highest IT oscillator strengths. For the benzenoid and heteroaromatic bridging ligands, the para- and ortho-substituted rings lead to more intense bands than the meta isomers. (2) For the isomers with the more intense bands, the intensity decreases with an increasing number of conjugated atoms in the bridging group. Thus, the oscillator strength decreases in the series L = pyrazine > 4CP > 14DCB > 15DCN. (3) The narrow, asymmetric near-IR bands are found only for the smallest bridges (pyrazine, NCCN, and N_2). (4) For L = 13DCA and 13DCB where the intermetal distances are the same but the nitriles are connected by saturated and unsaturated linkages, respectively, the IT bands have roughly the same intensity and energy.

Infrared Spectra. Binding of Ru^{II} to nitriles is known to shift the C≡N stretching frequency to lower energy,[30,31] in contrast

Table V. Intervalence Band Maxima, Widths, and Intensities for Bis(pentaammineruthenium(II,III)) Mixed-Valence Complexes[a]

bridge	ν_{max}/ ($cm^{-1} \times 10^3$)	$\Delta\nu_{1/2}$/ ($cm^{-1} \times 10^3$)	ϵ_{max} (corr)[b]	f^c
pym	7.15	6.00	41	1.1×10^{-3}
3CP	11.8	5.10	23	5.4×10^{-4}
4CP	10.7	5.17	1100	2.6×10^{-2}
12DCB	9.45	5.40	98	2.4×10^{-3}
13DCB	13.3	5.86	8	2.2×10^{-4}
14DCB	11.6	5.60	507	1.3×10^{-2}
15DCN	12.8	5.90	135	3.7×10^{-3}
16DCN	nd[d]			$<1 \times 10^{-4}$
17DCN	13[e]	6(est)	20	5.5×10^{-4}
26DCN	13[e]	6(est)	140	3.7×10^{-3}
27DCN	nd[d]			$<1 \times 10^{-4}$
13DCA	13.3	6(est)	12	3.3×10^{-4}
PPDCP	12.5	6(est)	10	2.8×10^{-4}
N≡N	9.8	2.63[f]	1400	1.8×10^{-2}
NCCN[g]	7.0	1.61[f]	410	3.0×10^{-3}
pyz[h]	6.4	1.25[f]	5000	3.7×10^{-2}

[a] In 1 M D_2SO_4/D_2O at room temperature. [b] In M^{-1} cm^{-1} (corrected for K_c). [c] By $f = 4.6 \times 10^{-9}$ $(\epsilon)(\Delta\nu_{1/2})$. [d] Not detected. [e] No distinct peak. [f] Band is asymmetric (see text). [g] Reference 10. [h] Reference 11.

Table VI. Nitrile Stretching Frequencies for Free Ligands and Ruthenium(II) Complexes[a]

ligand	ν_{CN} (free ligand)	ν_{CN} (Ru–L)	anion	shift ($\Delta\nu_{CN}$)
Binuclear Complexes				
12DCB	2238	2180[b]	$CF_3SO_3^-$	58
13DCB	2234[c]	2207[b]	$CF_3SO_3^-$	27
14DCB	2232[c]	2176[b]	$CF_3SO_3^-$	56
3CP	2232[c]	2200	PF_6^-	32
4CP	2243[c]	2190	ClO_4^-	53
15DCN	2235	2186	ClO_4^-	49
16DCN	2235	2180	ClO_4^-	55
17DCN	2236	2198	ClO_4^-	38
26DCN	2238	2198	ClO_4^-	40
27DCN	2240	2194	I^-	46
13DCA	2243	2228	ClO_4^-	15
PPDCP	2225	2180	Br^-	45
Mononuclear Complexes[c]				
benzonitrile	2231	2194	Br^-	37
acetonitrile	2254	2239	BF_4^-	15
14DCB	2232	2186	Br^-	46
4CP (CN bound)	2243	2179	Br^-	64
3CP (CN bound)	2232	2181	ClO_4^-	51

[a] Pentaammine and bis(pentaammine) complexes. All spectra taken at room temperature as KBr pellets. Frequencies in cm^{-1}. [b] From ref 27. [c] From ref 30 and 31.

to many other metal(II) nitrile complexes where the frequency is shifted to higher energy.[34] The nitrile ligands and their Ru^{II} complexes used in this study have been surveyed, and the results

(34) Nakamoto, K. "Infrared and Raman Spectra of Inorganic and Coordination Compounds", 3rd ed.; Interscience: New York, 1977; p 259.

Table VII. Electrochemical Data and Calculated Values of K_c for Ruthenium Binuclear Complexes[a]

ligand[b]	$E_{1/2}{}^{1}$ [c]	$E_{1/2}{}^{2}$ [c]	K_c[d]	electrolyte
pym	530	380	343	1 M HCl
	537[e]	391[e]	294	1 M HCl
12DCB	621	531	33.2	1 M HCl
	620[e]	532[e]	30.7	1 M HCl
13DCB	613	551	11.2	0.1 M CF_3SO_3H
14DCB	584	512	23.4	1 M HCl
	585[e]	509[e]	19.3	1 M HCl
3CP	649	424	6370	1 M CF_3SO_3H
4CP	684	409	45000	1 M CF_3SO_3H
15DCN	553	503	7.0	1 M HCl
	558[e]	508[e]	7.0	1 M HCl
16DCN	595	540	8.5	0.1 M CF_3SO_3H
17DCN	592	532	10	0.1 M CF_3SO_3H
26DCN	590	530	10	0.1 M CF_3SO_3H
27DCN	580	524	9	0.1 M CF_3SO_3H
13DCA	531	471	10	0.1 M CF_3SO_3H
PPDCP	573	535	~4	0.1 M CF_3SO_3H

[a] From cyclic voltammetry except where indicated otherwise. [b] General formula: $[(Ru(NH_3)_5)_2ligand]^{4+/5+/6+}$. [c] mV vs. NHE. [d] Values for K_c from cyclic and differential pulse width methods (ref 13). [e] From differential pulse.

are listed in Table VI. In all cases, the characteristic shift of ν_{CN} to lower energy is observed. Within isomeric groups, larger shifts are observed with the ortho,para type bridging ligands, and the aryl nitrile bridged complexes in general have larger shifts than found for L = 13 DCA. These differences are probably associated with the degree of Ru(II) $\rightarrow \pi^*$ back-bonding in the complexes,[35] which depends in part on the energy of the π^* acceptor orbital(s). For example, the lowest energy MLCT is substantially higher in energy for the acetonitrile Ru^{II} complex than that of the benzonitrile complex ($\Delta E = 17 \times 10^3$ cm^{-1}).[30] The energy of the MLCT band is closely related to the energy of the LUMO of the ligand.[36]

Electrochemistry. Electrochemical data and the values of K_c calculated from them (eq 1) are given in Table VII. Values of $E_{1/2}$ for each step in the reduction of [III, L, III]

$$[III, L, III] + e^- = [II, L III], E_{1/2}{}^1$$

$$[II, L, III] + e^- = [II, L, II], E_{1/2}{}^2$$

were obtained by application of theoretical results presented elsewhere.[12] Attempts to obtain K_c by the titration method of Sutton[2,5,28] usually gave irreproducible results, with the exception of L = 15DCN, where an average value of $K_c = 11$ was obtained for two determinations.[37]

Discussion

Electronic Description of Localized MV Complexes. The electronic spectra of the mixed-valence species [II, L, III] studied here have features attributable to the presence of both Ru^{II} and Ru^{III} in the complex. Moreover, the energies of the MLCT and LMCT transitions change very little from the isovalent to the mixed-valent state (Table II). Therefore, it is reasonable to regard the MV species as being localized on the time scale of electronic transitions.

Electronic and vibrational effects in class II mixed-valence systems have generally been considered separately, following a familiar practice in spectroscopy, where the usual procedure is to rewrite the transition moment as a product of electronic and Franck–Condon terms. The electronic transition moment between initial state i and final state f, μ_{if}, is weakly dependent on the nuclear positions. It is commonly assumed that μ_{if} is constant and equal to the calculated value at the equilibrium geometry, and the integrated intensity of a band is the sum of individual vibronic intensities. The total intensity of an electronic transition will then be closely approximated by μ_{if}.

Electronic effects in mixed-valence dimers will be considered here without explicit reference to the molecular vibrations or solvation. It will be shown that the role of the bridging ligand can be accounted for semiquantitatively when sufficient symmetry is present to allow separation of bonding metal orbitals (σd) from orbitals (πd) counted as nonbonding if the metal–bridge interaction is not considered. As shown by Xα calculations on $[Ru(NH_3)_6]^{2+,3+}$,[38] the πd orbitals in d^5 and d^6 ruthenium hexaammines are almost completely metal in character. Interaction between a ligand and d^6 Ru(II) will include πd–π^* delocalization when acceptor orbitals of π symmetry are available on the ligand, and the interaction is manifested in MLCT bands in the electronic spectrum. The π acceptor nature of Ru(III) is seen quite clearly in the observed LMCT bands. A symmetry match between donor, bridge, and acceptor orbitals is crucial if a simplified theory is to be successful. When the match is not present, distortions must occur to break the symmetry of the molecule. Such molecular distortions complicate treatment of the electronic problem.

The general technique to be used is based on superexchange theory.[40] The application of this approach to bridging ligand effects in intramolecular electron transfer was first suggested by George and Griffith[41] and later extended by Halpern and Orgel.[42] Superexchange theory has been widely used in explaining magnetic interactions in solids and polynuclear molecules.[43–45] More recently, Mayoh and Day[18–20] have applied the essentials of the Halpern and Orgel approach to the Creutz ion, $[(Ru(NH_3)_5)_2pyz]^{5+}$, and other MV systems. Although the validity of using perturbation theory for the Creutz ion has been questioned,[46] the approach is likely to be useful for weakly coupled MV dimers such as those studied here. Our equations are based on those of Mayoh and Day,[18–20] but a somewhat different expression is used to calculate intervalence band transition moments. The formal equations are presented first and are followed by a more qualitative discussion.

The ground state of a binuclear MV ion involves the distribution of electrons in the ion itself and the interaction between the ion and the solvent. The accurate calculation of such a state is an enormous task, but for our purposes it is not necessary to include explicitly the various contributions to the energetics of the system. Instead, the energy of the ground-state configuration is taken as zero, and the solvent and core electrons are taken into a general wave function ψ_0'. Also included in ψ_0' are bonding electron states and ligand electrons. In the course of excitation of the nonbonding πd electrons, it is simply assumed that ψ_0' does not change. We are concerned with metal and bridging ligand orbitals of π symmetry only, and it is assumed that only one πd orbital interacts (i.e., the ligand is planar), as shown:

(35) Ford, P. C. *Coord. Chem. Rev.* **1974**, *5*, 75.
(36) Lavallee, D. K.; Fleischer, E. B. *J. Am. Chem. Soc.* **1972**, *94*, 2583.
(37) The method of Sutton, Sutton, and Taube[5] for determining K_c via an intervalence band titration can be used in certain favorable cases. The original program for fitting the titration data was in nonstandard code, but has been converted to FORTRAN IV. A listing is available from the authors.
(38) Richardson, D. E.; Taube, H., unpublished results. Full details of SCF-Xα-scattered wave calculations on $[Ru(NH_3)_5]^{2+}$ and $[Ru(NH_3)_6]^{3+}$ are available in ref 23. The π4d orbitals (t_{2g} in O_h, but actually obtained as a_{1g} and e_g in D_{3d}) for both ions are found to be >80% localized within the Ru spheres (radius 3.976 au), an indication of minimal π interaction with ammonia. Similar conclusions are made by Ondrechen et al.,[39] who performed SCF-Xα-discrete variational calculations on the same species.
(39) Ondrechen, M. J.; Ratner, M. A.; Ellis, D. E. *J. Am. Chem. Soc.* **1981**, *103*, 1656.
(40) Kramers, H. A. *Physica (Amsterdam)* **1934**, *1*, 182.
(41) George, P.; Griffith, J. *Enzymes, 2nd Ed.* **1959**, *1*, 347.
(42) Halpern, J.; Orgel, L. E. *Discuss. Faraday Soc.* **1960**, *29*, 32.
(43) (a) Anderson, P. W. "Magnetism"; Rado, G. T., Suhl, H., Eds.; Academic Press: New York, 1963; Vol. 1, p 25. (b) Goodenough, J. B. "Magnetism and the Chemical Bond"; Interscience: New York, 1963. (c) Martin, R. L. "New Pathways in Inorganic Chemistry"; Ebsworth, E. A. V., Maddock, A. G., Sharpe, A. G., Eds.; Cambridge University Press: London, 1968.
(44) Ginsberg, A. P. *Inorg. Chim. Acta Rev.* **1971**, *5*, 45.
(45) van Kalkeren, G.; Schmidt, W. W.; Block, R. *Physica B+C (Amsterdam)* **1979**, *97B+C*, 315.
(46) Hush, N. S. *Chem. Phys.* **1975**, *10*, 361.

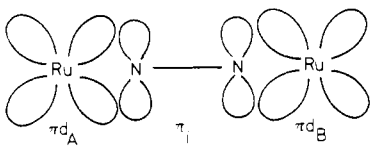

The L orbital π_i may be occupied or unoccupied and there is a total of three electrons in πd_A and πd_B. To zero order, the interaction between the πd_A, πd_B, and $L\pi_i$ are ignored. The interaction is later taken as a perturbation. The ground-state determinental wave function is then

$$\psi_0 = |d_A\bar{d}_A\pi_1\bar{\pi}_1...\pi_n\bar{\pi}_n d_B|\psi_0'$$

where two electrons are paired in d_A and an electron hole exists in d_B. There are a total $2n$ π electrons on the bridging ligand. An excited state can be written

$$\psi_1 = |d_A\bar{d}_B\pi_1\bar{\pi}_1...\pi_n\bar{\pi}_n d_B|\psi_0'$$

where the $\bar{d}_A$ electron is transferred to the $\bar{d}_B$ orbital. The state ψ_1 amounts to an intervalence charge-transfer state. The energy difference between ψ_0 and ψ_1 arises from nonequilibrium solvent polarization and bond distances in ψ_1. That is, ψ_1 represents an excited vibrational state created by vertical excitation from the ground state.[14-17] Thus there will usually be an energy difference between ψ_0 and ψ_1, although the *ground* states of the two configurations may be of equal energy (as would be true for a symmetrical binuclear MV ion).

There are other excited states now involving the ligand orbitals, e.g.,

$$\psi_2 = |d_A\bar{\pi}_1{}^*\pi_1\bar{\pi}_1...\pi_n\bar{\pi}_n d_B|\psi_0'$$

$$\psi_3 = |d_A\bar{d}_A\pi_1\bar{d}_B...\pi_n\bar{\pi}_n d_B|\psi_0'$$

corresponding to $d_A \rightarrow \pi_1{}^*$ and $\pi_1 \rightarrow d_B$ CT transitions, respectively. There will be several of these CT states, the total depending on the number of π orbitals on the ligand. Other states can be ignored: e.g., $\pi \rightarrow \pi^*$ ligand-centered transitions have little effect on metal–ligand and metal–metal interactions.[47]

Configuration interaction between the zero-order states will produce more accurate wave functions Ψ_0, Ψ_1, ..., where

$$\Psi_0 = \sum_j c_{0j}\psi_j \quad (2)$$

$$\Psi_1 = \sum_j c_{1j}\psi_j \quad (3)$$

and so on. The coefficients c can be obtained from perturbation theory. The requirement for the validity of the perturbational approach is that the interaction energy be small compared to the zero-order energy differences between ψ_0 and ψ_j (j = 1,2,...).

Each ligand π orbital is represented by a LCAO,

$$\pi_i = \sum_k a_{ik}\varphi_k \quad (4)$$

$$\pi_i{}^* = \sum_k a_{ik}{}^*\varphi_k \quad (5)$$

where π_i and $\pi_i{}^*$ are the occupied and unoccupied orbitals, respectively, and the a_{ik}, $a_{ik}{}^*$ are the coefficients of the 2p atomic orbitals φ_k. The approximate energies and coefficients for these ligand orbitals were calculated by an energy-corrected INDO method.[48]

(47) Consider, for example, a state created by promoting π_1 to $\pi_1{}^*$:

$$\psi_{\pi_1\rightarrow\pi_1{}^*} = |d_A\bar{d}_A\pi_1{}^*\bar{\pi}_1...\pi_n\bar{\pi}_n d_B|\psi_0'$$

It is easy to show that integrals of the one-electron operator h vanish in some cases, e.g.,

$$\langle\psi_1|h|\psi_{\pi_1\rightarrow\pi_1{}^*}\rangle = 0$$

The contribution from the electron repulsion operator $1/r_i$ is taken as zero in the zero differential overlap approximation. The effect of these results is that the ligand-based excited states do little to affect the interaction between ψ_0 and ψ_1.

Table VIII. Spectroscopic β_1 Values for Mixed-Valence Bis(pentaammineruthenium(II,III)) Complexes

bridging ligand	ν_{max}/ (cm^{-1} × 10^3)	μ/(e Å)	$\beta_1{}^a$/ (cm^{-1} × 10^3)	Δ^a/ (cm^{-1} × 10^3)
pym	21.9	0.96	8.71	20.3
pyz[b]	17.7	1.12	6.36	16.0
3CP	22.8	0.91	9.20	22.3
4CP	20.3	1.07	7.98	19.7
12DCB	22.5	0.66	6.35	22.2
13DCB	24.6	0.95	10.90	24.0
14DCB	21.5	1.10	9.55	20.8
15DCN	21.7	0.84	10.43	21.3

[a] By eq 8 and 9. [b] Creutz, C. Ph.D. Thesis, Stanford University, 1970.

Charge-Transfer Transitions. Charge-transfer processes involving the bridging ligand are important in considering the mechanism of bridge-mediated metal–metal interaction. To put the charge-transfer spectra on a semiempirical level, we use the simple Mulliken approach.[58] The basic equation for the transition moment is taken as

$$\mu_{0j} \simeq -(B_{0j}R_{ML})/\Delta_{0j} \quad (6)$$

where the subscripts refer to the ground state ψ_0 and excited state ψ_j, B is the appropriate resonance integral between the zero-order states ψ_0 and ψ_j, R_{ML} is the distance from the donor to the acceptor site, and Δ_{0j} is the energy difference between ψ_0 and ψ_j.

We now consider MLCT transitions ($Ru^{II} \rightarrow \pi^*$). If it is assumed that the metal–ligand interaction involves only the metal-bound atom (in this case N), the resonance integral is simplied via eq 5 and the assumption of zero differential overlap to

$$B_{0j} = \langle\pi d|\mathcal{H}|\pi_i{}^*\rangle = a_{iN}{}^*\langle\pi d|\mathcal{H}|\varphi_N\rangle \equiv a_{iN}{}^*\beta_{Ru^{II}\text{-}N} \equiv a_{iN}{}^*\beta_1 \quad (7)$$

where $\pi_i{}^*$ is the relevant acceptor orbital with an orbital coefficient of $a_{iN}{}^*$ at the nitrogen bound to Ru. In the case of a MLCT involving Ru^{II} and a π^* acceptor orbital, there are two optical electrons and a factor of $2^{1/2}$ is included in the transition moment. From eq 6 and 7,

$$\mu_{0j} = -\frac{2^{1/2}a_{iN}{}^*\beta_1 R_{ML}}{\Delta_{0j}} \quad (8)$$

in units of eÅ when R_{ML} is in Å. This expression is identical with that given earlier by Mayoh and Day.[18] If experimental values of μ_{0j} are known and $a_{iN}{}^*$ is calculated by the MO method, β_1

(48) We have chosen the INDO method,[49] but it became obvious in the course of the study that Hückel π orbitals would give reasonable results. While the coefficients derived by the INDO method give acceptable charge distributions, the orbital energies are known to be quite poor.[50-52] Since orbital energies enter rather prominently into the theory of bridge-related mediated interactions, a correction of the INDO orbital energies was made. When possible, experimental photoelectron energies were used for occupied π orbitals.[51-54] In other cases, an empirical correction was applied to the calculated energies. For unoccupied π orbitals, results of electron-resonance transmission spectroscopy measurements on related molecules[55-57] were used to correct the INDO energies empirically. Further details are found in ref 23.

(49) Dobosh, P. A. *QCPE* **1969**, *11*, 141.
(50) Kaufmann, J.; Presont, H.; Kerman, E.; Cusachs, L. *Int. J. Quantum Chem., Symp.* **1973**, *7*, 249.
(51) Rabalais, J. W. "Principles of Ultraviolet Photoelectron Spectroscopy"; Wiley: New York, 1976.
(52) Turner, D. W. "Molecular Photoelectron Spectroscopy"; Wiley-Interscience: London, 1970.
(53) Cyanopyridines: Kobayashi, T.; Nagakura, S. *J. Electron Spectrosc. Relat. Phenomen.* **1974**, *4*, 207.
(54) Dicyanogen: Hollas, J. M.; Sutherley, T. A. *Mol. Phys.* **1972**, *24*, 1123.
(55) Jordan, K. D.; Burrow, P. D. *Acc. Chem. Res.* **1978**, *11*, 341.
(56) Jordan, K. D., private communication, 1979.
(57) Nenner, I.; Schulz, G. J. *J. Chem. Phys.* **1975**, *62*, 1747.
(58) Mulliken, R. S.; Person, W. B. "Molecular Complexes"; Wiley: New York, 1969.

Table IX. Comparison of Theoretical and Experimental Parameters for Intervalence Bands[a]

bridging ligand	M-M distance[b]	μ_{IT}/(eÅ) calcd[c]	μ_{IT}/(eÅ) obsd[d]	c_{01}(eq 14)	c_{01}(eq 15)	V_{AB}/cm^{-1} [e]	$\lvert\rho_{NN'}\rvert$ [g]
pym	6.0	0.126	0.12	0.021	0.020	143	0.051
pyz[f]	6.9	0.67	0.66	0.096		3200	0.358
3CP	8.2	0.014	0.065	0.0017	0.0079	93	0.009
4CP	9.3	0.253	0.47	0.027	0.050	535	0.129
12DCB	5.9	0.073	0.15	0.012	0.025	236	0.053
13DCB	10.2	0.022	0.039	0.0022	0.0038	50	0.000
14DCB	11.8	0.142	0.32	0.012	0.027	314	0.050
15DCN	12.1	0.034	0.16	0.0028	0.013	169	0.009
16DCN	11.7	0.0002	<0.02	0.00002	<0.002		0.001
17DCN	8.1	0.032	0.062	0.0039	0.008	104	0.019
26DCN	14.0	0.092	0.16	0.0066	0.011	148	0.025
27DCN	12.8	0.005	<0.02	0.0004	<0.002		0.001
PPDCP	12.0	0.007	0.045	0.00054	0.0038	48	0.006
NCCN[f]	7.7		0.2		0.026	3500	0.568
NN[f]	5.0		0.41		0.082	4900	1.00
13DCA	10.2		0.048		0.0047	62	

[a] For bis(pentaammineruthenium(II,III)) binuclear complexes. [b] In Å, assuming a Ru-N distance of 2.0 Å. [c] By $\mu_{IT} = c_{01}R_{MM}$. [d] From $f = 1.085 \times 10^{-5}\ (\nu_{max})\mu^2$. [e] Calculated from experimental intensity by eq 15 and 16. [f] Mixed-valence complexes of these ligands are strongly coupled and eq 12 and 14 do not apply. The V_{AB} is taken as half the near-IR band energy. [g] Defined as $2\Sigma_i^n a_{iN}a_{iN'}$, where n is the number of occupied molecular orbitals on the bridge.

can be estimated by setting Δ_{0j} equal to the observed transition energy, $h\nu_{0j}$, as an initial guess. The energy of a charge-transfer transition is approximately

$$h\nu_{0j} = \Delta_{0j} + \frac{2(a_{iN}{}^*\beta_1)^2}{\Delta_{0j}} \tag{9}$$

and iterative substitution between eq 8 and 9 will result in consistent values for β_1 and Δ_{0j}. Values of β_1 and Δ_{0j} were obtained in this way from the lowest energy MLCT bands for several of the mixed-valence complexes (Table VIII) and selected monomeric Ru^{II}–π acid complexes (Table III). Values of β_1 are found to be in the range of 7000–10 000 cm^{-1}, with values for the nitriles being somewhat higher than those when N is heterocyclic. The shifts in the maxima to lower energy when Ru^{III} is bound to the Ru^{II}–L complexes are associated with increased stability of the acceptor energy level (i.e., decreasing Δ_{0j}). These shifts are due to the inductive effect of Ru^{III} and are most noticable for smaller ligands such as pym and 4CP.

The above analysis can in principle be applied to LMCT transitions associated with Ru^{III}–L interactions by removing the $2^{1/2}$ in eq 8. However, in the experimental spectra, the LMCT band energies and intensities are often difficult to obtain because of overlap with other bands. An analysis of a few monomeric and binuclear Ru^{III} complexes puts $\beta_{Ru^{III}L-N}$ ($\equiv\beta_2$) at roughly 6000–7000 cm^{-1}.

Intervalence Bands. The calculation of intervalence transfer (IT) band intensities involves the transition moment matrix element:

$$\mu_{IT} = \mu_{01} = \langle\psi_0|z|\psi_1\rangle \tag{10}$$

where the metal–metal axis is taken as the z axis. It can be shown that to a good approximation the sums representing Ψ_0 and Ψ_1 (eq 2 and 3) can be truncated at $j = 1$ for purposes of calculating m_{IT}. Therefore, μ_{IT} becomes

$$\mu_{IT} = \langle c_{00}\psi_0 + c_{01}\psi_1|z|c_{10}\psi_0 + c_{11}\psi_1\rangle \tag{11}$$

The coefficients c_{00} and c_{11} are expected to be close to unity. Again following Mulliken,[58] the approximate transition moment is then

$$\mu_{IT} \simeq c_{01}R_{MM} \tag{12}$$

where R_{MM} is the metal–metal distance. Evaluation of c_{01} is based on judicious use of empirical data. To second order, c_{01} is

$$c_{01} = \frac{1}{\Delta_{01}}\left(\langle\psi_0|\mathcal{H}|\psi_1\rangle + \sum_{j>1}\frac{\langle\psi_0|\mathcal{H}|\psi_j\rangle\langle\psi_j|\mathcal{H}|\psi_1\rangle}{E_j - E_0}\right) \tag{13}$$

where Δ_{01} is the zero-order energy difference between ψ_0 and ψ_1. By use of the zero differential overlap approximation, the first-order term in eq 13 is $\langle d_A|\mathcal{H}|d_B\rangle$ and represents the direct exchange term. At the metal–metal separations in question, ≥6 Å, this term will be negligible. The second-order term involves coupling of the configurations ψ_0 and ψ_1 via higher energy charge transfer states. This general mathematical form for through-bridge coupling has been suggested by a number of authors.[18-20,42,59,60] A typical ordering of energy levels for ruthenium ammines with organic π acids is $E_0 = 0$, $E_1 \simeq 10 \times 10^3$ cm^{-1}, $E_2 \simeq 20 \times 10^3$ cm^{-1} (πd–π^*), and $E_3 \simeq 35 \times 10^3$ cm^{-1} (πd–π).

When small perturbations of ψ_0 and ψ_1 occur, the energy difference Δ_{01} can be approximated by the intervalence band energy ($h\nu_{IT}$). Insertion of the wave functions ψ_j and eq 4 and 5 into eq 13 and application of the zero differential overlap approximation yields

$$c_{01} = \frac{\beta_1\beta_2}{h\nu_{IT}}\left(\sum_{i=1}^{m}\frac{a_{iN}{}^*a_{iN'}{}^*}{E_i{}^* - E_0} - \sum_{i=1}^{n}\frac{a_{iN}a_{iN'}}{E_i - E_0}\right) \tag{14}$$

where N and N′ are the nitrogens of the ligand bound to the metals. $E_i{}^*$ and E_i are the energies of the MLCT and LMCT zero-order states involving $\pi_i{}^*$ and π_i, respectively, and there are a total of n π orbitals and m π^* orbitals on the bridge. The reversal in sign for the second summation is due to the properties of the zero-order determinental functions $\psi_j (j = 0, 1, 2...)$. For simplicity, the product $\beta_1\beta_2$ is assigned the value of 60×10^3 cm^{-1} for all cases.

The energies $(E_i{}^* - E_0)$ and $(E_i - E_0)$ are approximated by the observed CT frequencies when possible and, otherwise, by combining observed CT energies with the corrected orbital energies from the INDO calculations. For example, if $(E_1{}^* - E_0)$ is observed at 25×10^3 cm^{-1}, $(E_2{}^* - E_0)$ is given by 25×10^3 cm^{-1} + $(e_2{}^* - e_1{}^*)$, where $e_1{}^*$ and $e_2{}^*$ are the orbital energies of the π^* one-electron states.

Calculation of μ_{IT} (eq 12) is done by using the value of R_{MM} obtained assuming Ru–L bond distances of 2.0 Å and normal dimensions for the bridge. A correction of $3^{1/2}$ is applied to account for the distribution of the electron hole in the $4d^5$ orbitals of Ru^{III}. This correction assumes equivalent occupancy of d_{xy}, d_{yz}, and d_{xy}, an assumption of dubious validity. It is likely, however, that the hole distributions for the chemically similar molecules studied here are fairly constant. The results are summarized in Table IX along with experimental moments. Considering the approximations of the theory, it is too optimistic to expect excellent agreement between the calculated and observed moments, but the values are quite close. Semiempirical methods

(59) Ulstrup, J. *Lect. Notes Chem.* **1979**, *10*.
(60) Ratner, M. A. *Int. J. Quantum Chem.* **1978**, *14*, 675.

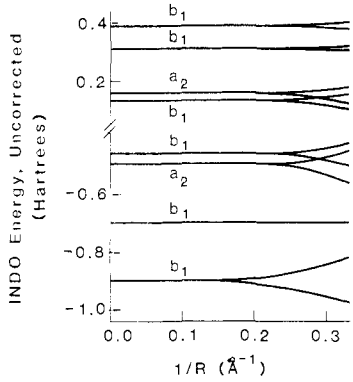

Figure 3. Variation of π orbital energies with inter-ring distance R for dibenzonitrile by INDO method.

often suffice to reveal the causes of observed trends, and that appears to be the case here.

Within isomeric groups, the direction and magnitude of changes in μ_{IT} for different isomers are reproduced. Ignoring for the moment what may be the improper use of the theory for [II, pyz, III] (vide infra), it is seen that the lower intensity for [II, pym, III] is predicted by the theoretical results (the almost exact agreement between theory and experiment is fortuitous). For the dicyanobenzene and cyanopyridine groups, where use of the theory is justified in all cases, the ortho and para isomers show higher μ_{IT} values in both theory and experiment. The difficulty in obtaining accurate IT data for the dicyanonaphthalenes makes comparison less meaningful, but the (1,5), (1,7), and (2,6) isomers are predicted to have the more intense bands. Experimentally, IT bands are observed only for these isomers. Although the IT bands in the (1,6) and (2,7) cases may be obscured by the visible MLCT bands, it is likely that they are much weaker than those of the other three isomers.

Because of the nonseparability of σ and π orbitals in 13DCA and DCBCO, no theoretical estimate can be made for the IT band intensities of [II, 13DCA, III] and [II, DCBCO, III]. Experimentally, the energy and intensity of the [II, 13DCA, III] band is very close to that of [II, 13DCB, III]. This reflects the inefficient coupling provided by meta-substituted aromatic rings. In contrast, the experimental moment for [II, 14DCB, III] is ~10 times greater than that of [II, DCBCO, III],[61] thus illustrating the efficiency of para coupling through aromatic rings.

The ligand PPDCP was modeled theoretically as dibenzonitrile with the structure

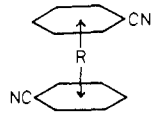

The distance R was varied from 3.0 to 5 Å to observe the effect of inter-ring distance on the calculated coupling. The dependence of the one-electron energies on R is shown in Figure 3. The inter-ring distance for [2,2]paracyclophanes is ~3.0 Å[62a] and for [3,3]paracyclophanes ~3.25 Å.[62b] The calculated μ_{IT} for [3,3]PPDCP is a factor of 33 less than the value for [2,2]PPDCP. Thus inter-ring coupling is a sensitive function of R in the range of 3.0–3.5 Å, as suggested by other studies.[63] At R = 5 Å, the molecular orbitals of dibenzonitrile are essentially those of isolated benzonitrile, and coupling in the dimer is predicted to be extremely weak. Coupling through the methylene linkages would probably become important at such an inter-ring distance. One can easily see the relationship of R to the theory (eq 14). As the rings separate, the orbital energies approach those of benzonitrile (Figure 3), and the excited states ψ_2, ψ_3, ...ψ_{n+2} begin to pair off into symmetric and antisymmetric combinations of benzonitrile orbitals. As R increases, there is an increasing cancellation of terms in eq 14 since the pair states are of opposite sign. At $R = \infty$, the pairs are degenerate and $\mu_{IT} = 0$, as one would expect intuitively. In reality, the coupling through the side linkages and lack of conformational rigidity would complicate the comparison of experiment to the calculations.

Although a calculated value of μ_{IT} for [II, pyz, III] is given in Table IX, the perturbational approach of eq 14 is probably not useful for modeling this MV ion. Strongly coupled MV ions such as [II, pyz, III],[11] [II, NCCN, III],[9] and [II, NN, III][1] have asymmetric transitions in the near-IR that are more closely related to excitation between delocalized molecular orbitals than the CT nature of IT bands in localized complexes.[1] Very strongly coupled and delocalized ions are better treated by a vibronic model of the type proposed by Schatz[17] or by molecular orbital theory.[1] The perturbational approach of eq 14 fails when the interaction energy between ψ_0 and ψ_1 is large compared to the zero-order splitting.

The treatment of bridging ligand effects presented thus far has followed the idea of superexchange first applied to electron transfer by Halpern and Orgel.[42] A second mechanism considered by these authors is double exchange. The interaction in double exchange involves movement of an electron to the bridge from the reducing center concomitant with motion of a bridge electron to the oxidizing center, and the interaction is found to be proportional to the mobile bond order between the ligand atoms bound to the metals. In Table IX, the bond orders, ρ_{NN}, are given for the bridging ligands. It is found that the same general ordering of μ_{IT} is predicted by the bond order and superexchange (eq 14) approaches.

It is difficult to assess the importance of double exchange in relation to superexchange. One would expect that states of all types (involving both occupied and unoccupied orbitals on the bridge) would contribute to the interaction. The orbital energies of the ligand orbitals are explicitly included in superexchange, and they are known to be important factors in the strength of metal–metal interactions. For example, creation of a high-energy π orbital by deprotonation of NCCRHCN leads to a large increase in metal–metal interaction in $[(Ru(NH_3)_5)_2NCCRCN]^{4+}$ sufficient to delocalize the MV complex.[8] In terms of a superexchange mechanism, this results from the relatively small energy difference between metal πd orbital and the HOMO of the deprotonated bridge. In eq 14, the second term would become larger as the energies become closer until the coupling becomes strong enough to delocalize the complex (when eq 14 no longer applies). The LMCT band in $[Ru(NH_3)_5NCC(tert\text{-butyl})CN]^{2+}$[27] at 12.7 $\times 10^3$ cm^{-1} gives an estimate of the πd – π energy difference.

Early in the study of ruthenium(II,III) mixed-valence complexes with π acceptor bridging ligands, it was often assumed that the LUMO of the bridge was the most important orbital in determining metal–metal coupling. The calculations based on eq 14 show that all π and π^* orbitals contribute significantly to the coupling interaction for a wide range of bridging ligands. This is because the energy terms $(E_i - E_0)$ and $(E_i^* - E_0)$ vary by a factor of only 2 or 3, while the resonance integrals generally have about the same value in all terms. Thus, is is usually incorrect to assume that either the LUMO or HOMO of the bridge determines the interaction. In some cases, perhaps exemplified by $[NCCRCN]^-$ above, one particular orbital may dominate in the interaction if it is unusually close in energy to the metal orbitals.

Metal–Metal Interaction Energy. The relationship between the intensity of an IT band and the actual interaction energy will now be considered. Several authors have shown the relationship between the interaction energy V_{AB} and band intensities in localized MV ions.[14,15,17] The distance between the metal centers must be considered in the comparison since large distances imply larger transition dipoles (eq 12). Thus the quantity directly related to the interaction energy is the coefficient given theoretically by c_{01}, and eq 15 has often been used.[14] In eq 15, ν and the halfwidth

$$c_{01}^2 = \frac{(4.24 \times 10^{-4})\epsilon_{max}\Delta\nu_{1/2}}{\nu_{max}R_{MM}^2} \qquad (15)$$

(61) Hammershoi, A., work in progress.

(62) (a) Hope, H.; Bernstein, J.; Trueblood, K. N. *Acta Crystallogr., Sect. B* **1972**, *B28*, 1733. (b) Gantzl, P. K.; Trueblood, K. N. *Acta Crystallogr.* **1965**, *18*, 958.

(63) (a) Weissman, S. I. *J. Am. Chem. Soc.* **1958**, *80*, 6462. (b) Ishitani, A.; Nagakura, S. *Mol. Phys.* **1967**, *12*, 1.

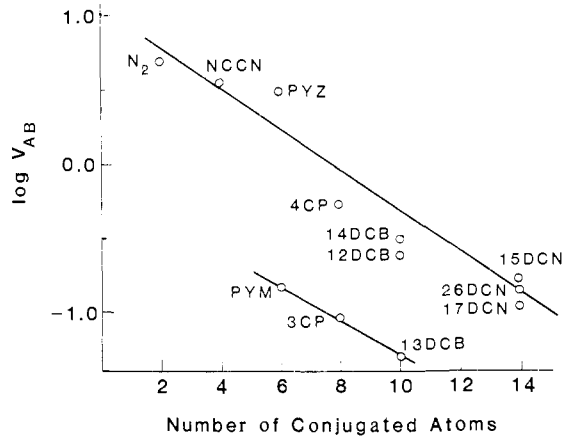

Figure 4. Plot of log V_{AB} (Table IX) vs. number of conjugated atoms in the bridging ligand.

$\Delta\nu_{1/2}$ are in cm^{-1}, ϵ is in M^{-1} cm^{-1}, and R_{MM} is in Å. The use of this equation has been strongly criticized by Wong et al.,[64] but it is recognized as a useful method for obtaining relative degrees of delocalization. The interaction energy is commonly given by the approximate expression[14,15]

$$V_{AB} = c_{01}\nu_{max} \tag{16}$$

where ν_{max} is the energy of the IT band maximum. Values of V_{AB} from experimental coefficients of delocalization are given in Table IX.

Rules for π-Mediated Interaction. A few guidelines for predicting the relative degree of metal–metal interaction in related intramolecular redox systems are now presented. These rules assume π-mediated interaction between donor and acceptor orbitals of π symmetry, as in low-spin Fe^{II}/Fe^{III}, Ru^{II}/Ru^{III}, and Os^{II}/Os^{III}.

(1) For coupling through conjugated bridges, the interaction energy will decrease exponentially with the number of conjugated atoms. This relationship was suggested by McConnell[65] in his study of electron exchange in biphenyl radicals. His derivation of the interaction energy is based on Hückel orbitals and is applicable to conjugated chains. The approximate result is

$$V_{AB} = \left(\frac{-2T^2}{D}\right)\left(\frac{-\beta_{CC}}{D}\right)^{n+1} \tag{17}$$

where β_{CC} is the carbon–carbon resonance integral for the bridge linkages, and D is the energy difference between the ground state and unperturbedd bridge orbitals ($D > \beta_{CC}$), and n is the number of atoms in the chain. The constant T is the interaction energy between the donor or acceptor orbital and the chain. Although this equation is only approximate, it does show the reasonable exponential dependence of V_{AB} on the number of atoms in the bridging group.

In Figure 4, the variation of the experimental interaction energies for the MV ions (as log V_{AB} from Table IX) are plotted against the total number of C and N atoms in the bridging ligands. A general exponential dependence is indeed observed, but the bridges are obviously divided into two groups: (1) those with an even or (2) those with an odd number of atoms separating the metal sites. Thus the meta isomers (L = pym, 3CP, 13DCB) follow a different line than the para isomers, but the two lines have about the same slope.

The dependence of V_{AB} on the number of atoms in the bridging ligand can be understood qualitatively in the following way. As the number of conjugated atoms increases, each gets less total charge density from back-bonding with Ru^{II}. The interaction of a given atom with Ru^{III} will then decrease roughly in proportion to the charge density at the binding site. Since an ortho, para, meta alternation effect for charge density is present in bridges containing rings, there will naturally be two groups of V_{AB}, depending on the substitution pattern of the rings (see rule 2 below).

(2) If a metal is bound to the starred position of a neutral alternating hydrocarbon bridging ligand, the strongest metal–metal interaction occurs when the second metal is bound at an unstarred position. For example, 3CP and 4CP are starred as shown:

and much stronger interaction is predicted for 4CP as a bridging ligand. This rule is clearly predicted by the double-exchange mechanism of Halpern and Orgel[42] and the superexchange expression of eq 14. The alternation effect is expected on the basis of general experience with the transmission of electronic effects through conjugated bond systems.

Observations for Ru^{II}–π acid monomers indicate that the charge redistribution from the metal involves principally the ortho and para positions. The effect is seen in pK_a data for pentaammineruthenium(II) complexes with π acids having two basic sites. For example, compare L = pym (pK_a(complex) = 0, pK_a(free ligand) = 1.3) and L = pyz (pK_a(complex) = 2.5, pK_a(free ligand) = 0.6).[29] The increase in basicity at the para position of pyz is easily explained by perturbation theory. As shown by Dewar,[66,67] $2e^-$ π donors (such as d^6Ru^{II}) on aromatic rings cause a negative charge increase in the π orbitals of the ground state almost exclusively at the ortho and para positions. The higher charge density on a nitrogen in the heterocycle results in increased basicity of the heterocycle.[36,68] These ideas provide a more intuitive rationale for the isomeric effects predicted by eq 14. The Ru^{II} density found at the ortho and para sites will interact to a greater degree with a Ru^{III} center at those positions, thus increasing V_{AB}.

(3) Coupling through extended saturated bridges will tend to be weaker than that through conjugated bridges of the same size. The relatively low interactions through saturated chains is partially due to the large energy separation of the chain orbitals and the metal valence levels. In eq 14, the energy terms in the denominator will be larger for saturated linkage, thus reducing the overall coupling. A second more subtle effect also operates when comparing saturated and unsaturated linkage. If the atoms of the bridging ligand that are bound to the metals interact weakly, then it is reasonable to expect a weak metal–metal interaction. For example, for bridging ligands of the type NCXCN, coupling is stronger when X is a benzene ring than when it is a methylene linkage (e.g., CH_2CH_2).[27] For 14DCB, the symmetric and antisymmetric combinations of the π levels on the nitriles are strongly split by their interaction with the ring. The same nitrile levels would be almost degenerate for X = CH_2CH_2. This near degeneracy would result in a substantial cancellation of terms in the sums of eq 14, since the terms would pair off into positive and negative terms of almost the same magnitude. More direct evidence for the relationship between intrabridge coupling and metal–metal interaction is reported by Stein[3] for dithioether bridging groups.

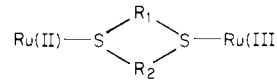

The metal–metal interaction (as approximated from the IT band intensity) was found to be correlated with the observed splitting of the sulfur lone pair binding energies found in the free ligand photoelectron spectrum.

(4) When the interaction is through stacked aromatic rings, V_{AB} will decrease exponentially with interplanar distance. This

(64) Wong, K. Y.; Schatz, P. N.; Piepho, S. B. *J. Am. Chem. Soc.* **1979**, *101*, 2793.
(65) McConnell, H. M. *J. Chem. Phys.* **1961**, *35*, 508.
(66) Dewar, M. J. S. "The PMO Theory of Organic Chemistry"; Plenum Press: New York, 1975.
(67) Dewar, M. J. S. *J. Am. Chem. Soc.* **1952**, *74*, 3341.
(68) Heilbronner, E. "The HMO Model"; Wiley: New York, 1975; p 396.

is an obvious prediction of the theoretical treatment in eq 8–14 and reflects the reasonable parallel of interaction energy with overlap integrals, which decrease exponentially with increasing interatomic distance. The ESR experiments of Weissman[63a] showed that electron exchange is rapid on the ESR time scale for the [2.2]paracyclophane anion but is slower for the [3.4], [4.4], and [6.6] cases. The decrease is partially due to the increased solvent trapping energy with increased interring distance, but interaction between the π electrons of the rings is certainly less for the latter cases and the effect observed may reflect a contribution from a nonadiabatic factor. Unfortunately, there is probably little chance of observing an intervalence transfer band directly when the rings are separated by more than 3.5 Å. In the present cases of Ru(II) nitrile lead-in groups, the strong CT absorbance in the visible region would probably obscure the IT band. In addition, lack of conformational rigidity would probably make direct observation of long-distance ring–ring interaction unlikely.

(5) Anionic organic bridges in which the electron pair is delocalized between binding sites will have relatively strong interaction; there is a general correlation between π acceptor strength and the interaction. An example of the former mechanism has been given, where the bridging anion is $[NCCRCN]^-$.[8,27] The large interaction arising with this bridging ligand is associated with its π donor characteristics, i.e., the energy difference between the HOMO of the bridge and the Ru^{III} acceptor orbital is relatively low (about $^1/_3$ the difference found for typical neutral conjugated organic ligands). Good π acceptors such as pyrazine, dicyanogen, and dinitrogen obtain much of the coupling energy via the π^* levels on the ligand although the π levels are also involved. Assuming an absence of direct metal–metal interaction, delocalized MV Ru^{II}–Ru^{III} complexes only occur with small bridges which are unusually strong π donors or π acceptors and feature complete delocalization of the occupied and/or unoccupied levels in the valence states. It is interesting to note that strong interaction tends to be associated with either relatively high-energy MLCT (e.g., L = N_2[1]) or low-energy LMCT (e.g., L = $[NCCRCN]^-$).

Bridging Ligand Effects in Intramolecular Electron Transfer. Many studies have been devoted to electron transfer between transition metals mediated by bridging groups[69,70] and some in which electron transfer is studied in the intramolecular mode.[70,71] Several in the latter class involve organic radicals.[63,72,73] An important motivation for this work has been to elucidate the effect on the redox rates of varying the bridging structure. The mixed-valence systems studied here provide an indirect way of investigating intramolecular redox phenomena. The relationship between the IT band energy and the classical activation barrier to electron transfer has been discussed elsewhere.[74] Here we will only consider the electronic effects resulting from variation of bridging ligand structure.

There is obviously some question about converting observed or theoretical IT band intensities into reliable interaction energies. The electron-transfer rates predicted by nonadiabatic theories[59,75–77] are based on Fermi's golden rule, where the square of the interaction energy partially determines the rate. The general expression for probability of passage from an initial vibronic level to a set of product levels is

$$W = \frac{4\pi^2}{h} V_{AB}^2 \rho \qquad (18)$$

where ρ contains the necessary Franck–Condon factors. For eq 18 to be useful, the interaction energy V_{AB} must be small compared to the spacing between the vibrational levels. Despite the difficulty in putting absolute energies for V_{AB} in eq 18, the relative rates for intramolecular electron tra;nsfer in very weakly coupled MV ions would be expected to follow the order of experimental IT band intensities (corrected for R_{MM}). Rates of thermal electron transfer in [Ru^{II}, Ru^{III}] MV ions have not yet been directly measured, apart from one case of a photochemically induced reaction.[78]

There is some indirect evidence from other experiments that suggests a rate dependence on bridging ligand size and geometry can be observed. The intramolecular Ru^{II}–L–Co^{III} systems[71] show a correlation of rate with the Ru^{II}–L–Ru^{III} IT band intensities and energies. Intramolecular electron transfer has been observed for several complexes of the type Co^{III}-$OC(O)R$-$NO_2^{\cdot-}$, where the nitro radical is produced by pulse radiolysis.[72] The decay rate to Co^{II} and CO_2–R–NO_2 is strongly dependent on the nature of R. For example, for R = phenylene, the decay rate of the para-substituted isomer is faster than that for the meta by a factor of 17, although the meta isomer is a somewhat stronger reductant. The direction of the isomer effect is just what would be predicted by the through-bridge model of eq 14. Thus, the idea that factors such as bridge size, orientation of substituents in conjugated bridges, interplanar distances, and saturation are important in intramolecular electron transfer is indirectly supported by our results.[79]

Bridging Ligand Structure and Comproportionation Constants. In an earlier report,[12] we outlined methods for estimating K_c from electrochemical data for binuclear compounds. The examples presented[12] were all symmetrical where the total site–site interaction (not to be confused with the electronic interaction energy V_{AB}) is obtained after correcting the observed $\Delta E°$ for the statistical contribution (35.6 mV).[80]

The majority of the symmetrical binuclear ions in Table VII can be classified as weakly interacting. The dicyanonaphthalene and PPDCP bridged molecules have K_c values that approach the statistical value of 4 (noninteracting). Since other effects can broaden cyclic peak-to-peak separation to some degree, values of $K_c \lesssim 10$ are probably within experimental error of 4. The other symmetrical species have values of K_c significantly greater than 4.

Several factors can contribute to the magnitude of K_c, and at the present time these can be treated only in an approximate manner. The more important factors are given below with an estimate of their importance. A more extensive discussion of (1) and (2) can be found elsewhere.[2,5]

(1) Electronic Delocalization. This quantity is probably quite small for the localized cases studied here. An estimate of its value[5] is given by $V_{AB}^2/h\nu_{IT}$, and the data in Tables IX and V leads to values in the range of 2 cm^{-1} (L = 13DCB) to 27 cm^{-1} (L = 4CP). At most, the effect of electronic delocalization on $\Delta E°$ is a few millivolts.

(2) Electrostatic Interaction. The inherent electrostatic stability of the MV state has been discussed in some detail elsewhere.[2,5] This is an important contribution to K_c in localized ruthenium ammine MV complexes, and the bridging ligand size is crucial in determining its magnitude (through R_{MM}).

(3) Increased π Acidity in the MV State. This contribution is observed with the smaller bridging groups such as pym, 12DCB, and 4CP. The presence of Ru^{III} on the bridge in the MV form causes an increase in the π acidity of the bridging ligand. This

(69) Taube, H.; Gould, E. *Acc. Chem. Res.* **1969**, *2*, 321.
(70) Haim, A. *Acc. Chem. Res.* **1975**, *8*, 264.
(71) Zawacky, S. K.; Taube, H. *J. Am. Chem. Soc.* **1981**, *103*, 3379.
(72) Whitburn, K.; Hoffman, M.; Simic, M.; Breznicik, N. V. *Inorg. Chem.* **1980**, *19*, 3180 and references cited therein.
(73) Harriman, J. E.; Maki, A. H. *J. Chem. Phys.* **1963**, *39*, 778.
(74) Meyer, T. J. In "Mixed Valence Compounds"; Brown, D. B., Ed.; Reidel: Dordrecht, 1980; p 75 and references therein.
(75) Levich, V. G. *Adv. Electrochem. Electrochem. Eng.* **1966**, *4*, 249.
(76) Jortner, J. *J. Chem. Phys.* **1976**, *64*, 4860.
(77) Kestner, N. R.; Logan, J.; Jortner, J. *J. Phys. Chem.* **1974**, *78*, 2148.
(78) Creutz, C.; Kroger, P.; Matsubara, T.; Netzel, T.; Sutin, N. *J. Am. Chem. Soc.* **1979**, *101*, 5442.
(79) A related discussion is given by Larrson, S. *J. Am. Chem. Soc.* **1981**, *103*, 4034.
(80) In two cases here (L = 3CP, 4CP), a different analysis applies since the microscopic potentials for the two sites are different. The approach used by Sokol et al.[81] shows that the observed potential difference $\Delta E°$ is defined by the difference in the microscopic potentials. It is impossible to separate the effects due to asymmetry from those resulting from the site–site interaction in a direct way. For highly asymmetric cases, the statistical factor is not important.
(81) Sokol, W. F.; Evans, D. H.; Niki, K.; Yagi, T. *J. Electroanal. Chem.* **1980**, *108*, 107.

increase is reflected in the shift of the MLCT band ($Ru^{II} \rightarrow L$) to lower energy than the monomeric or [II, L, II] cases (Tables II and VIII). A rough estimate of the increased stability of the MV state can be obtained from the observed MLCT band shifts. For example, if $\beta_1 = 8 \times 10^3$ cm^{-1} and Δ shifts from 20×10^3 to 19×10^3 cm^{-1} $\Delta E°$ will include perhaps 40 mV due to the π acidity effect. The estimate is made via eq 9 and assumes double occupancy of the relevant metal donor orbital.

(4) Interactions in the [III, L, III] or [II, L, II] States. For larger bridges, this should not be a factor. A direct test is the comparison of the MLCT band energies and shapes for the monomers and the fully reduced dimers [II, L, II]. The absence of significant changes indicates little instability in the [II, L, II] state. For smaller bridges, the balance of interelectronic repulsions on the metals and bridge with the stability due to $\pi d-\pi^*$ or $\pi d-\pi$ delocalization is difficult to quantify. The use of CT energies would be misleading in those cases since the mere presence of a metal center near the optical origin will perturb the band energy and shape.

(5) Structural Distortion. For bridging ligands studied here, the influence of the oxidation state of one metal center on the bonding at the other site is expected to be small. That is, the M-L bond lengths and angles in the MV state will be close to those found for normal Ru^{II} and Ru^{III} bonds.[82,83] Therefore, it is not expected that geometric distortion will be important here. When the coordination spheres for the two metal centers overlap, structural distortion can be an important factor in determining K_c.

Conclusions

The mixed-valence complexes chosen for this study serve to illustrate several aspects of the effect of bridging ligand structure on metal-metal interactions in polymetallic systems. Since the auxiliary ligand ammonia is innocent with respect to the πd orbitals, the observed trends are known to be associated almost completely with variations in the bridging groups. The trends are predicted theoretically in a straightforward way by combining a molecular orbital description of the bridging ligand with a semiempirical measure of metal-ligand charge-transfer interactions. While the perturbational approach is satisfactory for localized MV complexes, it is not applicable for very strongly interacting or delocalized cases. The relationship of bridging ligand size, orientation of substituents, interplanar distances, and saturation to metal-metal interaction has been demonstrated both theoretically and experimentally. Bridging ligand effects in intramolecular electron transfer reactions can be related to the present work via the interaction parameter V_{AB}.

Although the complexes studied here represent only one type of bridged MV system, many of the general ideas advanced can be applied to other related phenomena. For example, the question of the mechanism of electronic conduction in biological redox reactions is clearly open to the type of analysis used here. As more experimental data on redox reactions involving structurally characterized metalloproteins and model systems becomes available, possible redox "pathways" can be evaluated.

Acknowledgment. Support of this work by National Science Foundation Grant CHE79-08633 is gratefully acknolwedged.

Registry No. $[Ru(NH_3)_5pym](PF_6)_2$, 83708-86-5; $[[Ru(NH_3)_5]_2pym](PF_6)_4$, 83664-65-7; $[[Ru(NH_3)_5]_2pym]Cl_6$, 83664-66-8; $[[Ru(NH_3)_5]_23CP](PF_6)_4$, 83664-68-0; $[[Ru(NH_3)_5]_24CP](ClO_4)_4$, 83664-70-4; $[[Ru(NH_3)_5]_212DCB]Br_4$, 83664-71-5; $[[Ru(NH_3)_5]_213DCB](ClO_4)_4$, 83664-73-7; $[[Ru(NH_3)_5]_213DDB](BF_4)_4$, 83664-74-8; $[[Ru(NH_3)_5]_214DCB](CF_3SO_3)_4$, 83664-75-9; $[[Ru(NH_3)_5]_215DCN](ClO_4)_4$, 83664-76-0; $[[Ru(NH_3)_5]_216DCN](ClO_4)_4$, 83664-78-2; $[[Ru(NH_3)_5]_217DCN](ClO_4)_4$, 83664-80-6; $[[Ru(NH_3)_5]_226DCN](ClO_4)_4$, 83664-82-8; $[[Ru(NH_3)_5]_227DCN]I_4$, 83664-83-9; $[[Ru(NH_3)_5]_213DCA](ClO_4)_4$, 83664-85-1; $[[Ru(NH_3)_5]_2PPDCP]Br_4$, 83664-86-2.

(82) Richardson, D. E.; Walker, D. D.; Sutton, J. E.; Hodgson, K. O.; Taube, H. *Inorg. Chem.* **1979**, *18*, 2216.
(83) Gress, M. E.; Creutz, C.; Quicksall, C. O. *Inorg. Chem.* **1981**, *20*, 1522.

Crystal Structure of Vacuum-Dehydrated Silver Hydrogen Zeolite A

L. R. Gellens,* J. V. Smith, and J. J. Pluth

Contribution from the Centrum voor Oppervlaktescheikunde en Colloidale Scheikunde, B-3030 Leuven (Heverlee), Belgium, and the Department of the Geophysical Sciences, The University of Chicago, Chicago, Illinois 60637. *Received April 23, 1982*

Abstract: Crystals of zeolite 4A were fully exchanged with $AgNO_3$ solution and immersed in NH_4OH solution for 65 h. Electron microprobe analysis gave $Ag_{70}Si_{96}Al_{96}O_{384}\cdot xH_2O$, but the numbers are imprecise because of inadequate standards. A total of 26 H atoms would be needed for charge balance with 96 Al atoms. X-ray diffraction data for a crystal dehydrated at 410 °C and 10^{-5} torr were refined in space group $Fm\bar{3}c$ (a = 24.55 Å). The mean T-O distances (1.598 and 1.729 Å) are consistent with earlier evidence for alternation of tetrahedra populated by Si and $Al_{0.9}Si_{0.1}$. A total of 66 Ag atoms were located in four sites: 44 Ag(2) atoms near the center of a 6-ring, and bonded to 3 O(3) atoms at 2.28 Å; 7 Ag(3) atoms displaced from the center of an 8-ring and bonded to three oxygens at 2.4-2.9 Å; 6 Ag(1) atoms opposite a 4-ring inside the sodalite unit at 2.82 Å from 4 O(3) atoms; 9 Ag(2′) atoms displaced 0.5 Å from Ag(2) into the sodalite unit. The shortness of distances (2.95 and 2.92 Å) from Ag(1) to another Ag(1) and to Ag(2′) supports earlier evidence for the presence of a neutral or nearly neutral Ag atom at site 1. However, the size of possible clusters cannot be inferred because only one in eight of the type 1 sites is occupied. Electron density at the center of the sodalite unit would correspond to 0.9 Al atom, but the density for the corresponding oxygen was not located.

Introduction

Although the aluminosilicate framework of Al-rich zeolites collapses if complete hydrogen exchange is attempted,[1] partial exchange can be achieved in several ways. Heating after partial exchange with NH_4 results in liberation of NH_3 and formation of hydroxyl groups in the framework; however, vacuum extraction at 25 °C allowed dehydration without removal of NH_3.[2] An ion exclusion effect[3] allows replacement of Ag^+ by H^+; thus a single

* To whom correspondence should be addressed at the Katholieke Universiteit Leuven.

(1) Breck, D. W. "Zeolite Molecular Sieves"; Wiley: New York, 1974; p 569.
(2) McCusker, L.; Seff, K. *J. Am. Chem. Soc.* **1981**, *103*, 3441-3446.

0002-7863/83/1505-0051$01.50/0